Eur. Phys. J. A (2023) 59:139
https://doi.org/10.1140/epja/s10050-023-01050-3

THE EUROPEAN PHYSICAL JOURNAL A

New Tools and Techniques

Method to evidence hypernuclear halos from a two-target interaction cross section measurement

Simone Velardita[1,a], **Hector Alvarez-Pol**[2], **Thomas Aumann**[1,3,4], **Yassid Ayyad**[2], **Meytal Duer**[1], **Hans-Werner Hammer**[1,4], **Liancheng Ji**[1,4], **Alexandre Obertelli**[1,4], **Yelei Sun**[1,4]

[1] Technische Universität Darmstadt, Fachbereich Physik, Darmstadt 64289, Germany
[2] Universidade de Santiago de Compostela, Santiago de Compostela, 15782 Santiago, Spain
[3] GSI Helmholtzzentrum für Schwerionenforschung GmbH, Darmstadt 64291, Germany
[4] Helmholtz Forschungsakademie Hessen für FAIR, Frankfurt 60438, Germany

Received: 26 January 2023 / Accepted: 6 June 2023

Communicated by Takashi Nakamura

Abstract We present a two-target measurement method to determine the interaction cross section of hypernuclei with a target nucleus. The method allows to extract from two independent measurements the production cross section of a given hypernucleus as well as its interaction cross section on a specific target. The latter is then further analyzed to deduce the matter radius of the hypernucleus. The sensitivity of the method has been investigated for the specific case of the lightest hyperhalo candidate hypertriton ($^{3}_{\Lambda}$H) produced from ^{12}C+^{12}C collisions at 1.9 GeV/nucleon. Furthermore, its feasibility is demonstrated by detailed simulations for realistic experimental conditions at GSI/FAIR, using a dedicated HYDRA (HYpernuclei Decay at R^{3}B Apparatus) time-projection chamber prototype. A precision of 15% or better in the interaction cross section can be achieved, allowing an extraction of the unknown $^{3}_{\Lambda}$H matter radius and assessing its halo or non-halo character.

1 Introduction

Hyperons (Λ, Σ, Ξ, Ω) are baryons with at least one strange valence quark. The lightest hyperon, Λ, can only decay into a pion and a nucleon through the weak interaction, while the strong interaction conserves strangeness. The very short lifetime of hyperons (263 ps for the free Λ [1]) makes it technically extremely difficult to perform scattering or capture experiments with hyperon beams to study the hyperon-nucleon (*YN*) and hyperon-hyperon (*YY*) interactions. Few pΛ scattering data exist [2] and recent femtoscopy measurements provide new constraints on the bare *YN* and *YY* interactions [3,4]. Interestingly, hyperons can form bound systems with nucleons and create short-lived hypernuclei [5]. The extended exploration of the hypernuclear landscape opens a new area for nuclear structure and many-body baryonic interaction studies. Thanks to the absence of Pauli blocking with nucleons, a Λ hyperon can occupy any orbital inside the nucleus and can be used as a probe of the inner nuclear densities [6], barely accessible otherwise with the exception of electromagnetic probes only applicable to stable nuclei. The measured binding energies and energy differences between spin doublet states in hypernuclei give precise information on the *YN* interaction [7]. Study of *YY* interactions at saturation density is also expected by measuring the fine structure of double-Λ hypernuclei [8].

Hypernuclei presenting a halo have been predicted (see e.g. [9–12]). A nuclear halo is an intriguing quantum tunnelling phenomenon observed in nuclei at the dripline. The notable feature of halo nuclei is the large nuclear size due to the extended distribution of the halo nucleon(s) outside the region authorized by classical mechanics, typically larger than 50% probability [13]. The hypertriton $^{3}_{\Lambda}$H is an excellent candidate for a Λ halo in its ground state since the Λ is only bound by 130 $\pm$ 50(stat.) $\pm$ 40(sys.) keV [14] to a deuteron, a reference value from emulsion measurements. Meanwhile, a recent STAR measurement resulted in 410 $\pm$ 120(stat.) $\pm$ 110(sys.) keV [15], whereas a smaller value of 72 $\pm$ 63(stat.) $\pm$ 36(sys.) keV [16] was obtained by the ALICE collaboration. Due to the weak binding, the lifetime of $^{3}_{\Lambda}$H is expected to be not significantly different from that of the free Λ which is still under debate due to the dispersion of different measurements [16–20], although the most recent experimental value of 253 $\pm$ 11(stat.) $\pm$ 6(sys.) ps [16] by the ALICE collaboration is compatible with the free Λ lifetime. Unlike the halo in exotic nuclei, the spatial extension of hypernuclear

[a] e-mail: svelardita@ikp.tu-darmstadt.de (corresponding author)

Published online: 23 June 2023

halos has not been directly studied experimentally so far. It is expected that the glue-like role of a hyperon can facilitate the existence of hypernuclear neutron or proton halo state if the core nucleus is weakly unbound [10]. Two such interesting candidates are ${}^{6}_{\Lambda}$He (S_n = 0.17 MeV) and ${}^{7}_{\Lambda}$Be (S_{2p} = 0.67 MeV) [10]. Exploring these weakly bound hypernuclear systems can provide a unique opportunity to study the fundamental hyperon-nucleon interactions, which are not well constrained due to the lack of scattering data. New information on exotic hypernuclei would reveal facets of the *YN* and *YNN* interactions and would be an important benchmark for ab initio theories [21].

Light hypernuclear halos might be a key probe to understand the formation of nuclei in relativistic heavy-ion collisions, as currently performed at LHC with ALICE and at FAIR with CBM in the future. Indeed, coalescence models have been extensively used to describe the formation of composite objects (see e.g. [22–25]). Surprisingly, thermal-statistical models have been successful in describing the production of light (anti-)(hyper-)nuclei across a wide range of energies in A + A collisions [26,27]. The nucleosynthesis mechanism in relativistic ion collisions might be revealed by light halo hypernuclei under the condition that their basic features such as size and binding energy are known [28]. Indeed, thermal + blast-wave and coalescence models give very different predictions for the production of ${}^{3}_{\Lambda}$H as a function of the source size in the case ${}^{3}_{\Lambda}$H has an extended wave function. Therefore, it is essential to determine the hypertriton matter radius experimentally to be used as an input, and not a free parameter, in coalescence models. Predictions for the matter radius of hyperhalo ${}^{3}_{\Lambda}$H vary between 4–10 fm, depending on the binding energy. The structure of the hypertriton was studied within the pionless effective field theory (EFT), where a strong correlation between the binding-energy and its matter radius was found [29]. Considering the reference separation energy of 130 keV gives a matter radius of 4.9 fm. Lower binding-energy leads to higher values of the matter root mean square (rms) radius that can reach up to 10 fm [28].

Measuring the matter radius of hypernuclei is challenging for two main reasons: their low production cross section and their sub-nanosecond lifetime. Although there are different experimental methods to determine the matter radius of a nucleus, some of them require a high luminosity and are only applicable to stable nuclei, such as parity-violating electron scattering [30], or coherent photo-pion production [31]. Proton elastic scattering is in principle applicable to short-lived nuclei [32] but still requires beam intensities close to or above 10^4 particles per second (pps). In the case of very low intensities, the measurement of interaction or reaction cross sections of a projectile with an ion target can lead to a quantitative assessment on its matter radius. This was historically pioneered by Tannihata et al. for the two neutron-halo ^{11}Li [33]. Another observable being sensitive to a halo-like density tail of the wavefunction is the electromagnetic response or Coulomb cross section, as well known from studies of halo nuclei [34]. A quantitative prediction of the effect for the case of the hypertriton has been made recently in Ref. [35].

In the following, we present a method adapting the interaction-cross section measurement to hypernuclei. We demonstrate that a reasonable sensitivity to the interaction cross section can be achieved and give quantitative constraint on the matter radius of hypertriton.

2 The two-target method

2.1 General description

The method allows to measure the interaction cross sections of hypernuclei (${}^{A}_{\Lambda}$X) with a target nucleus and from these infer their matter radii. Hereby, the term 'interaction cross section' refers to all reactions that lead to a final state that is different from the initial hypernucleus in a bound state.

The population of hypernuclei inside the target region depends on two main processes: (i) the beam interacts with the primary target and according to the production cross section σ_Λ of the hypernuclei (unknown, since only few data with large uncertainties exist) a certain yield of hypernuclei is produced, (ii) this yield is then attenuated by the interaction with the target nuclei, according to the interaction cross section $\sigma_{\Lambda R}$ of the hypernucleus with the target (unknown) or decay according to its lifetime τ. To obtain the two unknown cross sections, it is proposed to perform two separate measurements. In principle, there are several experimental configurations that can be considered to reach this objective. The first possibility includes a single measurement using two targets of thicknesses, d_1 and d_2, separated by a flight gap L. This configuration requires less beam time since the measurement from both targets is done only once. However, distinguishing whether the primary vertex is allocated inside target 1 or 2 is technically challenging, and would require a high-granularity high-rate tracking detector placed in between the two targets. The second configuration introduces two independent measurements using the same beam and two targets of the same material but with increasing thickness. Although it requires a longer beam time, reconstruction of the decay vertex distribution (DVD) can be obtained with high accuracy as it is done with two independent measurements. The third configuration includes two independent measurements using the same target but two different beams with different hypernuclei production cross-section. It requires a long beam time and since the hypernuclei production cross section is low ($\sim \mu$b) such an option would require a measurement with a production cross section significantly lower than the other, i.e., extremely beam-time consuming. For these rea-

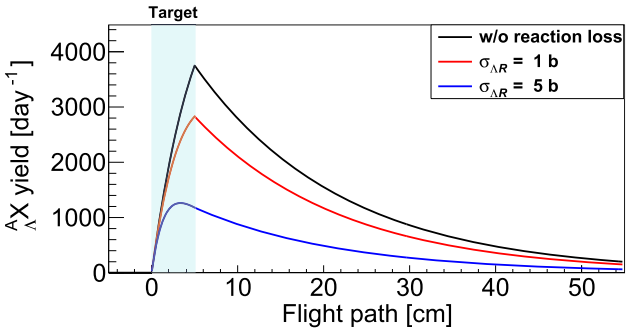

Fig. 1 Yield of hypernucleus $^{A}_{\Lambda}$X along the flight path assuming different interaction cross sections (different curves), and a ^{12}C beam at 1.9 GeV/nucleon with intensity of 10^6 pps impinging on a carbon target of thickness $d = 5$ cm (blue shaded band)

sons, we focus here on a method based on two separate measurements with identical beam and with two different target thicknesses of the same material, which will allow to access both σ_Λ and $\sigma_{\Lambda R}$. For simplicity, the interaction cross section of projectile-like hypernucleus ($^{A}_{\Lambda}$X) with a target (^{A}Y) can be expressed by the geometrical cross section

$$\sigma_{\Lambda R} = \pi[\mathrm{R}(^{A}_{\Lambda}\mathrm{X}) + \mathrm{R}(^{A}\mathrm{Y})]^2\,, \tag{1}$$

where $R(^{A}Y) = R_0\,A^{\frac{1}{3}}$ and $R_0 = 1.25$ fm. For the $^{3}_{\Lambda}$H, the interaction cross section will be analysed in Sect. 2.3 within the eikonal formalism to obtain a microscopic connection to its matter radius.

Hypernuclei produced will be reconstructed via the invariant-mass method by measuring the weak decay products in the final state. The observable that will be used to determine the interaction cross section is the mesonic DVD along the flight path downstream the target. The sensitivity of the DVD to $\sigma_{\Lambda R}$ (and consequently to the matter radius) is demonstrated in Fig. 1 for a generic hypernucleus, assuming: τ =200 ps, $\sigma_\Lambda = 1.8\,\mu$b (see Sect. 2.3) and different interaction cross sections $\sigma_{\Lambda R} = 0$ b, 1 b, 5 b. A sudden drop in the DVD can be seen due to the interaction downstream the target.

Below, a description of the method is presented, as well as its sensitivity for the specific case of $^{3}_{\Lambda}$H by an estimate of the uncertainties of its interaction cross section.

2.2 Analytical formulation

In the following, the second experimental configuration will be analyzed: the first measurement is done using only one cylinder of thickness d_1 and a second one with two cylinders of thicknesses, d_1 and d_2, separated by a flight gap L. For L=0, this corresponds to two independent measurements with a target thickness d_1 and a target of thickness $d_1 + d_2$. Assuming that all particles propagate along the beam axis (z), the population $N(z)$ of beam particles and $N_\Lambda(z)$ of hypernuclei can be formulated analytically:

$$\begin{cases} \mathrm{d}N(z) = -\,\delta\Big(n\sigma_R N(z)\Big)\mathrm{d}z\,, \\ \mathrm{d}N_\Lambda(z) = -\,\dfrac{N_\Lambda(z)}{\gamma\beta c\tau}\mathrm{d}z + \delta\Big(n\sigma_\Lambda N(z) - n\sigma_{\Lambda R} N_\Lambda(z)\Big)\mathrm{d}z\,, \end{cases} \tag{2}$$

where $\delta = 0, 1$ (0 in free space and 1 inside a target), σ_R is the reaction cross section of the beam projectiles with the targets, n the number density of the targets, β the velocity of the $^{A}_{\Lambda}$X in the laboratory frame, γ its Lorentz factor, τ its lifetime and c the speed of light. The boundary conditions are $N_\Lambda(0) = 0$ and $N(0) = N_0 = I \cdot t$, where I is the beam intensity and t is the total measurement time.

Once the DVD of $^{A}_{\Lambda}$X along the beam axis (z) has been extracted, it is of particular interest to extrapolate the populations at the exit of the targets, where the contribution from their interaction is the largest, this corresponds to $N_\Lambda(d_1)$ from the first measurement and $N_\Lambda(d_1 + L + d_2)$ for the second one. These two quantities can be analytically calculated using the set of equations defined in Eq. 2. By taking the ratio between the two populations, we eliminate the explicit dependence on σ_Λ. Re-arranging the terms one gets the following analytical formulation of the $^{A}_{\Lambda}$X interaction cross section:

$$\begin{aligned} &A\,(1 - e^{-B(\sigma_{\Lambda R})\,d_1})e^{-\left(\frac{L}{\gamma\beta\tau c} + B(\sigma_{\Lambda R})\,d_2\right)} \\ &- A\,e^{-B(\sigma_{\Lambda R})\,d_2} + e^{-B(\sigma_{\Lambda R})\,d_1} + A - 1 = 0\,, \end{aligned} \tag{3}$$

where, to help the readability of the equation, the following substitutions have been used

$$B(\sigma_{\Lambda R}) = n\sigma_{\Lambda R} + \frac{1}{\gamma\beta c\tau} - n\sigma_R\,,$$

$$A = \frac{N_\Lambda(d_1)\;N_{0,d_2}}{N_\Lambda(d_1 + L + d_2)\;N_{0,d_1}} \cdot e^{-n\sigma_R\,d_2}\,,$$

$N_{0,d_1} = I \cdot t\,\alpha$ is the number of beam projectiles that impinge on the first target ($z = 0$) for the first measurement, $N_{0,d_2} = I \cdot t\,(1 - \alpha)$ is that on the second target ($z = d_1 + L$) for the second measurement and α represents the share of the total beam time among the two measurements, i.e., $0 < \alpha \leq 1$. Note that the ratio between the two populations is contained in variable A, while the processes that affect the hypernuclei populations are contained in the function $B(\sigma_{\Lambda R})$.
In addition, for the case $L = 0$, Eq. 3 can be re-written as:

$$e^{-B(\sigma_{\Lambda R})\,d_1} - A\,e^{-B(\sigma_{\Lambda R})\,(d_1 + d_2)} - 1 + A = 0\,, \tag{4}$$

where $A = \dfrac{N_\Lambda(d_1)N_{0,d_2}}{N_\Lambda(d_1 + d_2)N_{0,d_1}} \cdot e^{-n\sigma_R\,d_2}$.

2.3 Sensitivity in the case of ${}^{3}_{\Lambda}$H+^{12}C at 1.9 GeV/nucleon

The sensitivity of the method is investigated for the case of the hypertriton (${}^{3}_{\Lambda}$H), where the considered production and decay channels are ^{12}C + ^{12}C $\rightarrow$ X + ${}^{3}_{\Lambda}$H and ${}^{3}_{\Lambda}\mathrm{H} \rightarrow {}^{3}\mathrm{He} + \pi^-$ (branching ratio, $BR = 26\%$ [36]), respectively. As presented in Sect. 1, it is of particular interest to study the size of ${}^{3}_{\Lambda}$H, the lightest predicted hyperhalo. In such a case, we cannot consider here the traditional geometrical interaction cross section of hypernucleus (Eq. 1), since the hypertriton is expected to be a dilute object for which the black-disk limit may not be suited. Instead, the correlation between the measured interaction cross section and the matter radius of ${}^{3}_{\Lambda}$H will be analysed with microscopic wave functions and the eikonal formalism, valid at the considered incident energies, beyond the simplistic geometrical ansatz.

The required inputs for the calculation are (i) the density distribution of ^{12}C, (ii) the density distributions of the Λ and the deuteron in the center of mass of ${}^{3}_{\Lambda}$H, (iii) proton-neutron and proton-proton total cross sections, (iv) Λ-nucleon total cross sections. Nucleon-nucleon cross sections at energies of $\sim$ 2 GeV have been measured [37], and the density distribution of ^{12}C can be considered well known, in particular, its charge density distribution from precision (e, e) measurements [38]. The neutron density distribution can be considered identical, as a good approximation. The Λ-nucleon total cross sections have been measured [39,40] and show a flat behaviour over a large range of energies. The measured values, fitted over momentum p in GeV/c, of $\sigma(\Lambda p) = (34.3 \pm 1.5)$ mb $- p^{-1}(-3.8 \pm 17.6)$ mb GeV/c and $\sigma(\Lambda n) = (34.1 \pm 3)$ mb $- p^{-1}(33 \pm 35)$ mb GeV/c are close to the nucleon-nucleon total cross sections. Note that at the energies relevant in this paper, the total cross section is expected to reflect the size of the colliding baryons, and show little momentum dependence (less than 1%), consistent with the above mentioned measurements. The radial density distributions for the neutron, proton and Λ in hypertriton are taken from theory. In the case of the pionless EFT, the rms radius of ${}^{3}_{\Lambda}$H can be tuned by modifying the Λ separation energy, as illustrated in [29]. We provide here the results for such calculations for hypertriton separation energies of 50 keV (rms radius = 7.9 fm from pionless EFT), 130 keV (rms radius = 4.9 fm) and 410 keV [15] (rms radius = 2.8 fm). The obtained cross sections are 1062 mb, 861 mb and 645 mb, respectively. In this section, the different predictions of the ${}^{3}_{\Lambda}$H matter radius, and consequently interaction cross section ($\sigma_{\Lambda R}$), will be analyzed considering detection efficiency $\varepsilon_{det} = 100\%$ for the weak decay products, where in the next section realistic conditions are considered.

The statistics of the experiment plays a fundamental role in the proposed method and determines the choice of the beam and targets. For the purpose of this sensitivity study, we consider realistic beam conditions at GSI/FAIR [41]: beam intensity $I = 10^6$ pps, beam energy $E_{beam} = 1.9$ GeV/nucleon, and a total beam time $t = 1$ day. At this energy the measured reaction cross section ^{12}C+^{12}C equals $\sigma_R = 888 \pm 19$ mb [42]. The method is general and applicable to other beams and different energies under the condition that it is above the Λ production threshold of 1.6 GeV/nucleon (elementary process $NN \rightarrow \Lambda K N$). In terms of the experimental setup, the parameters taken into consideration are: the target thicknesses (d_1 and d_2), the flight gap (L), and the share of total beam time among the two measurements (α). The mean free path of ^{12}C in the target is calculated to be $\lambda = 1/(\sigma_R n) = 10$ cm. In the case of a pronounced halo, the mean free path of the hypertriton is expected to be also in the order of 10 cm, which therefore, limits the maximum target thicknesses to avoid too many reactions. We analyze the contribution of these parameters to the uncertainty of the $\sigma_{\Lambda R}$ ($\delta\sigma_{\Lambda R}$) considering a lifetime $\tau({}^{3}_{\Lambda}\mathrm{H}) = 223^{+12}_{-11}$ ps [43]. The trend of the figures presented in this section is not affected by the choice of the lifetime, therefore the conclusions drawn from the method will remain unchanged. Note that Eq. 3 cannot be solved analytically, therefore the numerical bisection method [44] was used.

Figure 2 shows the resulted relative uncertainty of $\sigma_{\Lambda R}$ ($\delta\sigma_{\Lambda R}/\sigma_{\Lambda R}$) as a function of the target thicknesses for different matter radii. In the case of $L = 0$ and $\alpha = 50\%$ a minimum is reached, where the lowest values of $\delta\sigma_{\Lambda R}/\sigma_{\Lambda R}$ are obtained using a thin target for the first measurement, $d_1 \sim 3$ cm, and a thicker target for the second one, $d_1 + d_2 \sim 8 - 11$ cm. The values of $d_1 = 3$ cm for the first measurement and $d_1 + d_2 = 11$ cm for the second one will be used in this section.

The top panel of Fig. 3 shows the dependence of $\delta\sigma_{\Lambda R}/\sigma_{\Lambda R}$ as a function of α, considering $L = 0$, where a minimum is reached for $50\% \leq \alpha \leq 70\%$. The bottom panel of Fig. 3 shows the trend of $\delta\sigma_{\Lambda R}/\sigma_{\Lambda R}$ as a function of the flight gap (L) for a fixed $\alpha = 50\%$. The introduction of a gap between the two targets will only degrade the uncertainty as the yields of ${}^{3}_{\Lambda}$H will be reduced due to its decay.

To conclude, the optimal configuration obtained with the proposed method is: no gap between the two targets ($L = 0$), same boundary conditions of the beam for the two measurements $\left(N_0^{(1)} = N_0^{(2)}\right)$, and a large difference between the two target thicknesses. Specific values for the last parameters cannot be given as they strongly depend on the experiment, and therefore have to be evaluated accordingly.

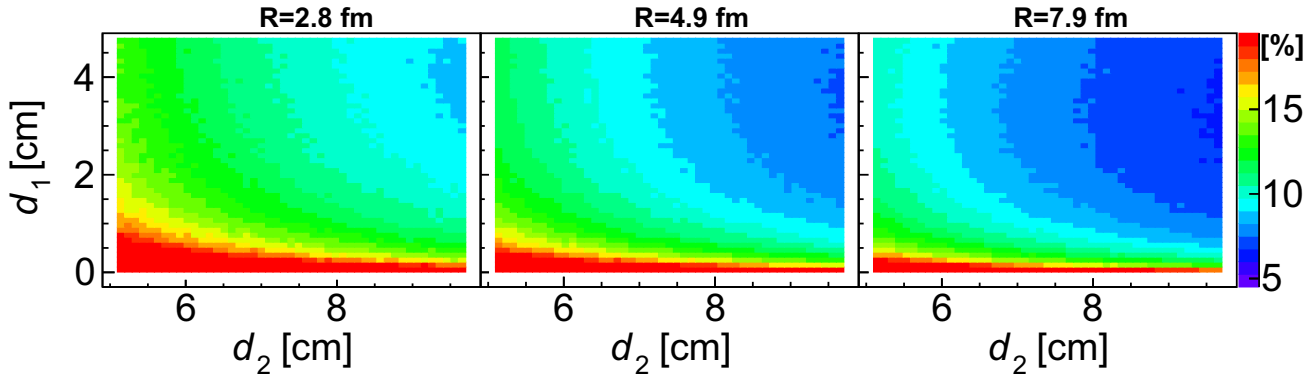

Fig. 2 Relative uncertainty of hypertriton interaction cross section ($\delta\sigma_{\Lambda R}/\sigma_{\Lambda R}$) with ^{12}C for several matter radii as a function of the target thicknesses d_1 and d_2, for $L = 0$ and $\alpha = 50\%$

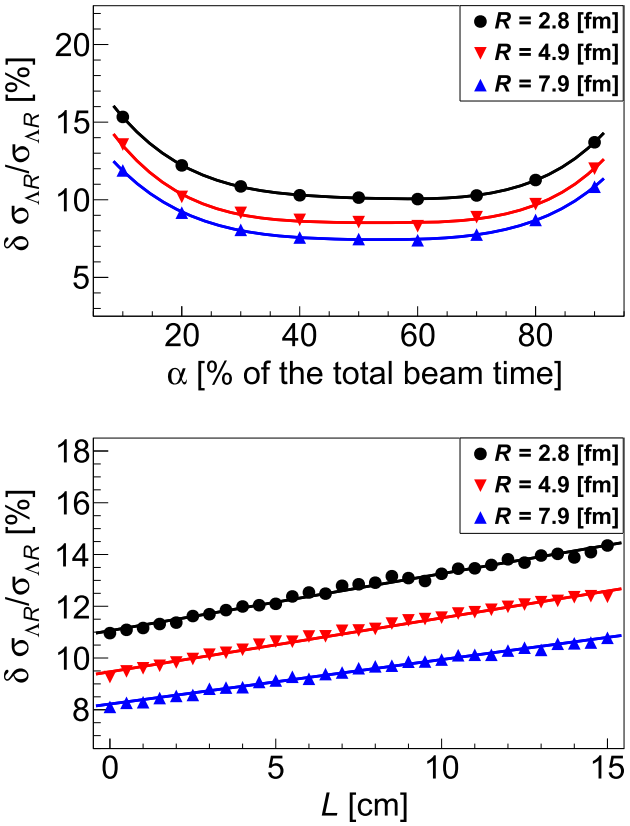

Fig. 3 Top: relative uncertainty of hypertriton interaction cross section ($\delta\sigma_{\Lambda R}/\sigma_{\Lambda R}$), considering $L = 0$, $d_1 = 3$ cm and $d_1 + d_2 = 11$ cm, for several hypertriton radii for a given amount of total beam time (1 day) as a function of α. Bottom: ($\delta\sigma_{\Lambda R}/\sigma_{\Lambda R}$) as a function of the flight gap L, considering $\alpha = 50\%$

3 Realistic implementation of the method: HYDRA at R^{3}B

3.1 Proposed experimental setup

The technique of using relativistic heavy-ion collisions to produce hypernuclei was first introduced in 1973 [45]. Since then, it has been exploited with light ions at several facilities [46–48]. The R^{3}B (Reactions with Relativistic Radioactive Beams) setup at GSI/FAIR has the potential for a world-unique contribution to the study of Λ-hypernuclei using relativistic stable and radioactive beams [49,50]. Radioactive ion beams with kinetic energy above the production threshold of 1.6 GeV/nucleon can be transmitted by the current fragment separator FRS ($B\rho_{max}$ = 18 T · m) and the next-generation fragment separator Super-FRS ($B\rho_{max}$ = 20 T · m) in the future. In the example presented in this paper a stable beam of ^{12}C is considered.

Since light hypernuclei decay via pion (π^-) emission, a dedicated setup providing sufficient acceptance and efficiency for low rigidity pions is required. Here, we introduce such a new experimental approach for kinematic-complete measurements, based on the detection of π^- by a dedicated time-projection chamber (TPC) from the decay of hypernuclei produced in heavy-ion collisions on a production target. The TPC is named HYDRA, standing for HYpernuclei Decay at R^{3}B Apparatus, where its prototype is shown in the bottom panel of Fig. 4: it is 1/3 the size of the full detector, with an active area of 88 × 256 mm^2 and has a drift region of 300 mm long. In addition to the TPC, a plastic wall behind the exit window of the TPC is employed as a start of the drift time measurement and for triggering. Decayed fragments (^{3}He for $^3_\Lambda$H) can be measured by scintillator fibers and plastic array (TOFD) in R^{3}B standard setup. The production targets, HYDRA prototype TPC and two additional fiber detectors, to determine the ion residue trajectories following the decay of hypernuclei, will be installed inside the GLAD magnet [51] of the R^{3}B setup, see Fig. 4 (top) for a schematic view of the experimental setup at R^{3}B.

The first hypernuclear experiment to be performed at R^{3}B focuses on the determination of the interaction cross section (and consequently the matter radius) of the hypertriton, using the two-target method introduced in this paper. The production and decay channels are the same introduced in

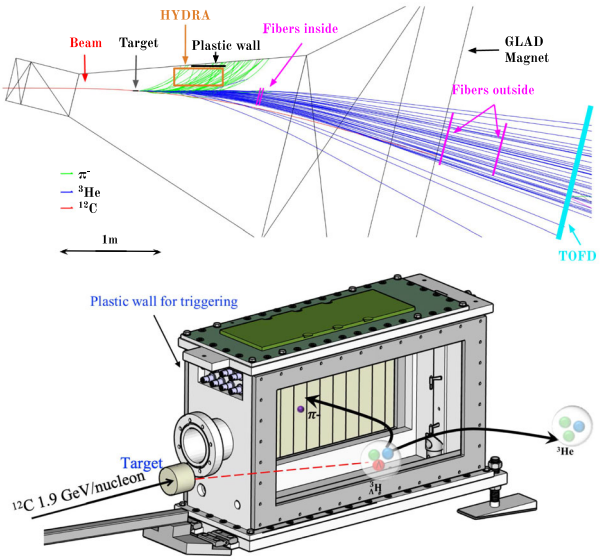

Fig. 4 Top: schematic of the experimental setup at R^{3}B for invariant-mass spectroscopy of hypernuclei. Simulated trajectories correspond to weak decay events of ${}^3_\Lambda$H into π^- (green) and ^{3}He (blue) after being produced from ^{12}C+^{12}C collisions at 1.9 GeV/nucleon. Positions of the detectors are optimized for the invariant-mass resolution and efficiency. Bottom: sketch of the HYDRA TPC prototype geometry and the experimental concept. The TPC aims at measuring π^- from the mesonic decay of light hypernuclei. The trajectory of the π^- is deflected in the GLAD magnetic field of around 2 T

the previous section, $^{12}\mathrm{C} + {}^{12}\mathrm{C} \rightarrow \mathrm{X} + {}^3_\Lambda\mathrm{H}$ and ${}^3_\Lambda\mathrm{H} \rightarrow {}^3\mathrm{He} + \pi^-$, respectively. Realistic experimental conditions impose several limitations that cannot be neglected and are discussed in this section. The beam configuration which will be used is: ^{12}C with $I = (1-5)\cdot 10^6$ pps (trigger rate limitation, see below), $E_{beam} = 1.9$ GeV/nucleon (maximum energy accessible currently at GSI), and $t = 8$ days (to ensure sufficient statistics). Since the production cross section of the hypertriton is predicted to be very low 1.8 μb [50], high intensity beam, $\mathcal{O}(10^6$ pps) is necessary. Combined with a thick target, this will lead to a high production rate of secondary particles and consequently a high trigger rate. Monte-Carlo simulations (using INCL++ [52] for fragmentation and the Dubna cascade model [53] for hypernuclei production) for a 6-cm thick ^{12}C target and beam intensity of 10^6 pps result in a trigger rate (coincidence between the trigger wall and TOFD, see Fig. 4) of 30 kHz. This is at the limit of the possible accepted rate by the R^{3}B setup, and as a consequence, the maximum target thickness has to be fixed to $d_{max} = 6$ cm. With this condition, the minimum uncertainty for the interaction cross section is obtained using $d_1 = 1$ cm and $d_2 = 5$ cm.

In the previous section, the detection efficiency has been neglected, i.e., assuming $\varepsilon_{det} = 100\%$. Here, several factors have to be taken into account: (i) detection efficiency of the π^- in the TPC 29%, (ii) detection efficiency of the fragment in the tracking detectors 60%, (iii) dead time, spill structure and acceleration duty 40%, (iv) analysis loss 20%.

3.2 Background estimate and measurement sensitivity

The produced hypertritons are tagged and identified by the invariant mass from their weak decay channel π^-+^{3}He. However, the interaction of the ^{12}C beam with the two carbon targets used for the measurement can produce a π^- and a ^{3}He ion which do not emerge from the decay of ${}^3_\Lambda$H, and can therefore lead to background in the invariant-mass spectrum. The possible background contributions are: (1) the coincidence of π^- and ^{3}He both produced from the fragmentation of ^{12}C, (2) the decay of a heavier hypernucleus which decays via pion emission together with a multi-ion final state that includes ^{3}He, and (3) a π^- from the decay of a free Λ, a K^0_S or a heavier hypernucleus and ^{3}He produced in coincidence from the fragmentation of the ^{12}C projectile. The following estimate does not take into account the two-step strangeness production, i.e., the production of hypertriton from fragments with $A \geq 3$ and $E_{kin} > 1.6$ GeV/nucleon formed in the primary collision. The maximal number of ${}^3_\Lambda$H produced from such a two-step process was estimated as 3% of the total amount of ${}^3_\Lambda$H produced by the primary interaction and is therefore neglected. In order to estimate this upper limit the following assumptions have been made: (i) all fragments are produced at the entrance of the target, (ii) the fragments with $A \geq 5$ have a production cross section of 1 μb, while for $A < 5$ are estimated from Ref. [50] which gives values smaller than 1 μb.

The background from (1) can be mostly removed by selecting the decay vertex position upstream the target [50]. The other two sources of background involve a weak decay, and therefore the pion emission outside the target as in the case of hypertriton decay. The background from (2) was quantified assuming a mesonic decay of the heavier hypernucleus, followed by the Fermi breakup of the decayed heavy residue. The relative kinetic energy between π^- and ^{3}He from such background will be always few MeV smaller than 43 MeV, that is the Q-value for the decay of ${}^3_\Lambda$H and therefore it is well separated from the invariant mass spectrum and the effect of background (2) can be considered as negligible.

The main source of background in the invariant-mass spectrum comes from (3). These background events can be reduced by requiring that (i) the tracks of the detected decay pion and ^{3}He intersect (5-mm minimum distance between the two tracks), (ii) the obtained decay vertex is outside the target by more than 10 mm, (iii) the distance between the reconstructed hypertriton track and the beam trajectory is within 5 mm, (iv) kinetic energy of the reconstructed hypertriton

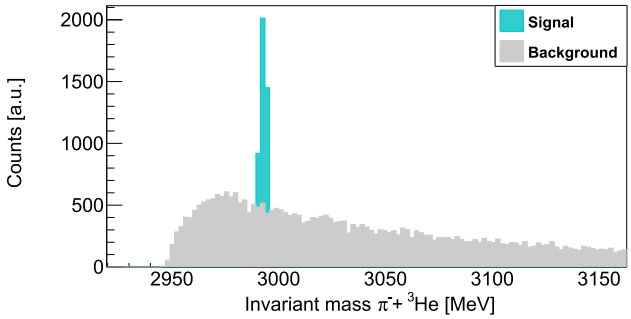

Fig. 5 Simulated invariant-mass spectrum of ${}^{3}_{\Lambda}$H for 8 days of beam time on target (see text for details)

should be less than 1.8 GeV/nucleon, determined through a comparison of the mixed events background and simulated signal distribution. The above cuts result in a signal over background of ∼3 see simulated spectrum in Fig. 5, while reducing the statistics of good events by 20%. The primary factors that contribute to the reduction are (i) and (ii), which are based on estimation of the vertex reconstruction precision described below. Yet, to test the sensitivity we varied the values by a factor of 2, i.e., setting (i) to less than 10 mm and (ii) to greater than 5 mm. The resulted signal over background ratio will decrease by a factor of 2.

In the simulation, we estimate an invariant-mass resolution of 2 MeV (sigma) based on the momenta of $\pi^- + {}^3$He. In particular, the pion measurement in the TPC is challenging and requires a dedicated reconstruction algorithm, suited for non-homogeneous magnetic field such as that of the GLAD magnet. Therefore, to be conservative, the simulation results presented in this section have been obtained assuming a vertex resolution of 5 mm. A full simulation for precise reconstruction vertex algorithm is currently under development, and further details are provided below.

The reconstruction of kinematics from the tracks recorded by the HYDRA TPC can be realized using a sequential process that includes track finding and fitting. Particles traversing the TPC will ionize the gas producing ionization electrons that are drifted to the segmented TPC pad plane. Using the pixel (pad) position and the drift velocity of the electrons, tracks can be reconstructed in three dimensions obtaining a collection of points in the space representing the track (hit pattern).

From the Langevin description of the drift, which takes into account the non-uniformity of the GLAD magnetic field, the electrons drift velocity and diffusion are calculated and applied to each electron. The procedure results in a three-dimensional hit pattern reflecting the pad plane information, which represents the real trajectories of the particles in TPC. The fitting of the individual trajectories uses a pattern recognition algorithm based on clusterization that assigns each particle track a collection of points of the hit pattern. Once this is achieved, they can be fitted to extract the kinematics from the track curvature and the energy loss using the so-called Kalman filter [54].

Table 1 Interaction cross sections for ${}^{3}_{\Lambda}$H with ^{12}C using Eq. 4, assuming two independent measurements with 1-cm and 6-cm thick carbon targets. Uncertainties from statistics and background subtraction are considered

Radius (rms) [fm]	$\sigma_{\Lambda R}$ [mb]	$\delta\sigma_{\Lambda R}/\sigma_{\Lambda R}$ [%]
2.8 (no halo)	645 ± 106	17
4.9	861 ± 129	15
7.9	1062 ± 134	13

An example of the application of the filter fitting for charged particle tracks in the range of momentum of interest can be found in Ref. [55]. The algorithm provides a resolution for the transverse momentum of (1-2)% for deuterons and tritons, close to the limits imposed by the spatial resolution and multiple scattering. In addition, a Runge–Kutta representation of each track can be used to extrapolate the track back to the target position out of the TPC and reconstruct the vertex with an intrinsic resolution of about 2 mm (standard deviation).

The GENFIT package [56], which offers a complete Kalman filter fitter has been implemented within the analysis flow for HYDRA. Preliminary results for the reconstruction of simulated π^-'s at 800 MeV/c with a homogeneous magnetic field of 2 T yield a momentum resolution of the order of 0.6%, adequate for inferring the kinematics of the reaction channel of interest.

Overall, using the HYDRA prototype, a precision of 15% or better for the interaction cross section, in the case of halo hypertriton, can be reached for $d_1 = 1$ cm and $d_1 + d_2 = 6$ cm, within 8 days of beam time at $\sim (1-5)\cdot 10^6$ pps, see Table 1 for details. In the HYDRA pioneering experiment, the main limitation arises from the reduced size of the TPC prototype. To compensate for this loss in efficiency, all other experimental conditions are maximized, in the limits of the experiment feasibility. In the future, more precise measurements can be achieved using the full-size TPC and an optimize setup accordingly.

4 Conclusions

We presented here an experimental approach to extract the interaction cross section of hypernuclei with a target nucleus via a two-target measurement. Performing two separate measurements with both thin and thick targets of the same material gives access to the production cross section of hypernuclei, poorly known to date, and their unexplored interaction cross section.

As a proof-of-principle, we performed a detailed study for the specific case of the lightest hyperhalo candidate ${}^{3}_{\Lambda}$H produced from ^{12}C+^{12}C collisions at 1.9 GeV/nucleon. The sensitivity of the method was investigated using a full simulation of realistic experimental configuration at R^{3}B (GSI/FAIR). The measurement principle is based on the weak decay channel of ${}^{3}_{\Lambda}$H into π^-+^{3}He via the invariant mass with high resolution. For the pioneering experiment foreseen at R^{3}B, we demonstrate that the interaction cross section of a halo hypertriton can be determined with a precision of 15% or better, mainly limited by statistics. When analyzed within the eikonal formalism, the interaction cross section is linked to the matter radius, thus allowing to assess the predicted halo nature of ${}^{3}_{\Lambda}$H.

Acknowledgements This work was supported by the German Federal Ministry of Education and Research - BMBF project numbers 05P21RDFN2 and 05P21RDFNB, the State of Hesse within the Research Cluster ELEMENTS (Project ID 500/10.006), the Alexandre von Humboldt foundation, as well as the Helmholtz Forschungsakademie Hessen für FAIR, Germany.

Funding Information Open Access funding enabled and organized by Projekt DEAL.

Data Availability Statement This manuscript has no associated data or the data will not be deposited. [Authors' comment: This manuscript does not report on a measurement.]

References

1. P.A. Zyla et al., PTEP, **2020**(8), 083C01 (2020)
2. J. Haidenbauer et al., Nuc. Phys. A **915**, 24–58 (2013)
3. ALICE collaboration. Phys. Rev. C **99**, 024001 (2019)
4. ALICE collaboration. Phys. Lett. B **797**, 134822 (2019)
5. M. Danysz, J. Pniewski, The London, Edinburgh, and Dublin Philosophical Magazine. J. Sci. **44**(350), 348–350 (1953)
6. A. Gal et al., Rev. Mod. Phys. **88**, 035004 (2016)
7. K. Tanida et al., Phys. Rev. Lett. **86**, 1982–1985 (2001)
8. https://panda.gsi.de/oldwww/archive/public/panda_loi.pdf (2004)
9. K. Miyagawa et al., Phys. Rev. C **51**, 2905 (1995)
10. E. Hiyama et al., Phys. Rev. C **53**, 2075–2085 (1996)
11. H.T. Xue et al., Phys. Rev. C **106**, 044306 (2022)
12. Y. Zhang et al. Prog. Theor. Exp. Phys. **023D01** (2022)
13. K. Riisager, The euroschool lectures on physics with exotic beams, vol. ii. pages 1–36 (2006)
14. M. Jurič et al., Nuc. Phys. B **52**, 1–30 (1973)
15. STAR Collaboration, Nat. Phys. **16**(4), 409–412 (2020)
16. ALICE Collaboration. https://arxiv.org/pdf/2209.07360.pdf (2022)
17. C. Rappold et al., Nuc. Phys. A **913**, 170–184 (2013)
18. ALICE Collaboration. Phys. Lett. B, **754**, 360–372 (2016)
19. STAR Collaboration, Phys. Rev. C **97**, 054909 (2018)
20. STAR Collaboration, Phys. Rev. Lett. **128**(20), 202301 (2022)
21. R. Wirth, R. Roth, Phys. Lett. B **779**, 336–341 (2018)
22. S.T. Butler, C.A. Pearson, Phys. Rev. **129**, 836–842 (1963)
23. H. Sato, K. Yazaki, Phys. Lett. B **98**(3), 153–157 (1981)
24. K. Blum et al., Phys. Rev. D **96**, 103021 (2017)
25. W. Zhao et al., Phys. Rev. C **98**, 054905 (2018)
26. A. Andronic et al., Phys. Lett. B **697**(3), 203–207 (2011)
27. A. Andronic et al., Nature **561**, 321–330 (2018)
28. F. Bellini, A. Kalweit, Phys. Rev. C **99**, 054905 (2019)
29. F. Hildenbrand, H.-W. Hammer, Phys. Rev. C, **100**, 034002 (2019). *Phys. Rev. C* **102**:039901, (2020), (erratum)
30. D. Adhikari et al., Phys. Rev. Lett. **126**, 172502 (2021)
31. C.M. Tarbert et al., Phys. Rev. Lett. **112**, 242502 (2014)
32. G. D. Alkhazov et al., Phys. Rev. Lett. **78**, 2313–2316 (1997)
33. I. Tanihata et al., Phys. Rev. Lett. **55**, 2676–2679 (1985)
34. T. Aumann, T. Nakamura, Phys. Scr. **2013**(T152), 014012 (2013)
35. C.A. Bertulani, Phys. Lett. B **837**, 137639 (2023)
36. W. Glöckle et al., Nucl. Phys. A **639**(1), 297c–306c (1998)
37. W.-M. Yao et al., J. Phys. G: Nucl. Part. Phys. **33**, 1–1232 (2006)
38. I. Sick, J.S. McCarthy, Nucl. Phys. A **150**, 631–654 (1970)
39. D. Bassano et al., Phys. Rev. **160**, 1239–1244 (1967)
40. S. Gjesdal et al., Phys. Lett. B **40**, 152–156 (1972)
41. GSI. Gsi helmholtz centre for heavy ion research. http://www.gsi.de
42. J. Jaros et al., Phys. Rev. C **18**, 2273–2292 (1978)
43. P. Eckert et al., https://hypernuclei.kph.uni-mainz.de (2021)
44. L. Richard, *Burden and J Douglas Faires*, 4th edn. (PWS-Kent Publishing Company, Boston, 1989)
45. A.K. Kerman, M.S. Weiss, Phys. Rev. C **8**, 408–410 (1973)
46. K.J. Nield et al., Phys. Rev. C **13**, 1263–1266 (1976)
47. S. Avramenko et al., Nucl. Phys. A **547**(1), 95–100 (1992)
48. C. Rappold et al., Nucl. Phys. A **913**, 170–184 (2013)
49. C. Rappold, J. López-Fidalgo, Phys. Rev. C **94**, 044616 (2016)
50. Y.L. Sun et al., Phys. Rev. C **98**, 024903 (2018)
51. B. Gastineau et al., IEEE Trans. Appl. Supercond. **20**(3), 328–331 (2010)
52. S. Leray et al., J. Phys. Conf. Ser. **420**, 012065 (2013)
53. V.D. Toneev, K.K. Gudima, Nucl. Phys. A **400**, 173–189 (1983)
54. R. Emil Kalman, Trans. ASME J. Basic Eng, **82**(Series D):35–45 (1960)
55. J.W. Lee et al., NIM A: Accelerators Spectrom. Detect. Assoc. Equip. **965**, 163840 (2020)
56. J. Rauch, T. Schlüter, J. Phys. Conf. Ser. **608**(1), 012042 (2015)